Title: The furin cleavage site in the SARS-CoV-2 spike protein is required for transmission in ferrets

Author list: Thomas P. Peacock[1#], Daniel H. Goldhill[1#], Jie Zhou[1#], Laury Baillon[1#], Rebecca Frise[1#], Olivia C. Swann[1], Ruthiran Kugathasan[1], Rebecca Penn[1], Jonathan C. Brown[1], Raul Y. Sanchez-David[1], Luca Braga[2], Maia Kavanagh Williamson[3], Jack A. Hassard[1], Ecco Staller[1], Brian Hanley[4], Michael Osborn[4], Mauro Giacca[2], Andrew D. Davidson[3], David A. Matthews[3], and Wendy S. Barclay[1*].

Affiliations:

[1]Department of Infectious Diseases, Imperial College London, UK, W2 1PG.

[2]British Hearth Foundation Centre of Research Excellence, School of Cardiovascular Medicine & Sciences, King's College London, UK, SE5 9RS

[3]School of Cellular and Molecular Medicine, Faculty of Life Sciences, University of Bristol, UK, BS8 1TD

[4]Department of Cellular Pathology, Northwest London Pathology, Imperial College London NHS Trust, UK, W6 8RF

# - these authors contributed equally to this work

*Corresponding author: tel: +44 (0)20 7594 5035, email: w.barclay@imperial.ac.uk

Word limits:

Abstract: 204/200

Introduction: 405/500

Main body: 3590/3750 (excluding methods)

Abstract

SARS-CoV-2 entry requires sequential cleavage of the spike glycoprotein at the S1/S2 and the S2' cleavage sites to mediate membrane fusion. SARS-CoV-2 has a polybasic insertion (PRRAR) at the S1/S2 cleavage site that can be cleaved by furin. Using lentiviral pseudotypes and a cell-culture adapted SARS-CoV-2 virus with an S1/S2 deletion, we show that the polybasic insertion endows SARS-CoV-2 with a selective advantage in lung cells and primary human airway epithelial cells, but impairs replication in Vero E6, a cell-line used for passaging SARS-CoV-2. Using engineered spike variants, live virus competition assays and measuring growth kinetics we find that the selective advantage in lung and primary human airway epithelial cells depends on the expression of the cell surface protease TMPRSS2, which enables endosome-independent virus entry by a route that avoids antiviral IFITM proteins. SARS-CoV-2 virus lacking the S1/S2 furin cleavage site was shed to lower titres from infected ferrets and was not transmitted to cohoused sentinel animals unlike WT virus. Analysis of 100,000 SARS-CoV-2 sequences derived from patients and 24 human post-mortem tissues showed low frequencies of naturally occurring mutants that harbor deletions at the polybasic site. Taken together our findings reveal that the furin cleavage site is an important determinant of SARS-CoV-2 transmission.

Main text

In 2019, SARS-CoV-2 entered the human population and by March 2020 was declared a pandemic by the WHO[1-3]. Coronaviruses enter host cells via their spike glycoprotein which is synthesised as an inactive precursor that must be cleaved to mediate membrane fusion. Depending on the sequence of spike at the S1/S2 junction the cleavage can occur either; i) during trafficking in the producer cell by host furin-like enzymes, ii) by serine-proteases such as the transmembrane protease, serine 2 (TMPRSS2) at the cell surface during attachment, or iii) by cathepsin proteases in the late endosome/endolysosome[4,5]. Upon S1/S2 cleavage and engagement of the host cell receptor with the spike receptor binding domain (RBD), a second cleavage site (CS) becomes exposed within the S2 domain, termed the S2' site[6-8]. Upon S2' site cleavage by serine proteases or cathepsins the S2 fusion peptide is liberated and initiates viral-host membrane fusion[7,9].

Like the closely related SARS-CoV, the cognate receptor of the SARS-CoV-2 spike is angiotensin-converting enzyme 2 (ACE2)[1,10]. While the SARS-CoV S1/S2 junction is well characterised as being cleaved by serine proteases or cathepsins, the SARS-CoV-2 spike, similarly to the more distantly related Middle Eastern respiratory syndrome-related coronavirus (MERS-CoV), contains a polybasic CS, characterised as being a suboptimal furin CS[6,11-13]. This polybasic CS is absent from the closest relatives of SARS-CoV-2, although similar polybasic CS are found in more distantly related coronaviruses[14-16]. It has been demonstrated for both MERS-CoV spike and SARS-CoV-2, that the furin CS at the S1/S2 junction promotes entry into lung cells[17-19], and that the furin CS contributes to viral pathogenesis in SARS-CoV-2 animal models[20,21]. SARS-CoV-2 has been repeatedly shown to rapidly lose this polybasic CS upon passage in Vero cells, a popular cell line for isolating and propagating the virus[22-28]. In addition, there are isolated reports of CS mutants sequenced directly from clinical swabs[22,24]. Several different mutants in this region are described including total deletions of the CS, loss of arginine substitutions within the CS making it less polybasic, or deletions

of flanking regions leaving the polybasic tract intact but potentially affecting accessibility to protease.

In this study, we use a combination of lentiviral pseudotypes with spike CS mutations and Vero passaged SARS-CoV-2 virus variants to investigate the molecular mechanism by which the polybasic CS of SARS-CoV-2 mediates efficient entry into lung cells. We describe the biological consequences of these mutations and test the effect of these mutations on viral transmission in ferrets.

Results

The polybasic S1/S2 cleavage site of SARS-CoV-2 spike protein allows cleavage during virus packaging

To investigate the importance of the spike polybasic CS of SARS-CoV-2 (PRRAR), a number of spike mutants predicted to modulate the efficiency of furin cleavage were generated (Figure 1a) including: substituting two upstream arginines to produce a monobasic CS similar to SARS-CoV spike (monoCS), replacing the tribasic CS with the furin CS of a highly pathogenic H5N1 avian influenza haemagglutinin containing seven basic amino acids (H5CS), and two naturally occurring deletions seen following passage in Vero E6 cells and/or in clinical isolates[21,26]. The first deletion removes eight amino acids including all 3 arginines of the PRRAR site (ΔCS), while the other removes five flanking amino acids but retains the tribasic CS (Δflank). The mutations were engineered into a spike expression plasmid to enable cell surface expression and generation of coronavirus lentiviral pseudotypes (PV). In addition, to study the importance of the PRRAR motif in the context of live virus we used a naturally occurring Vero cell-adapted mutant SARS-CoV-2, ΔCS[26]. This variant and the wild type virus from which it was derived were cloned by limiting dilution to enable studies using individual genotypes.

Furin cleavage of coronavirus spike proteins has been shown to correlate with syncytia formation when spike is overexpressed at neutral pH[7,18,29]. Therefore, we transiently expressed the SARS-CoV-2 mutant spike proteins in Vero E6 cells, which do not express TMPRSS2[30,31], and syncytia formation was compared to SARS-CoV and MERS-CoV spikes. As described before[18], SARS-CoV spike expression resulted in poor syncytia formation while MERS-CoV spike produced appreciable levels of syncytia (Figure 1b, Extended Data Figure 1). SARS-CoV-2 WT spike gave an intermediate level of syncytia formation that was ablated in the monoCS or ΔCS/Δflank mutants. The H5CS spike bearing the optimised furin CS produced a higher level of syncytia formation than SARS-CoV-2 WT, similar to MERS-CoV.

To investigate the differences in spike cleavage efficiency in producer cells between the mutants, PV with each mutant spike protein were concentrated and probed by western blot (Figure 1c, left panel). Equal amounts of PV particles were loaded as indicated by p24 content. Anti-spike S2 antibody detected two bands in PV, consistent with cleaved and uncleaved spike. For PV expressing WT SARS-CoV-2 spike, the stronger band corresponded to the cleaved S2 product. H5CS spike was more efficiently cleaved while SARS-CoV WT spike and SARS-CoV-2 monoCS and deletion mutants were largely uncleaved. Consistent with PV, authentic SARS-CoV-2 virus harboured both uncleaved and cleaved S2 whereas ΔCS mutant virus only contained uncleaved spike (Figure 1d). Overall, these data are consistent with previous work that has shown the polybasic CS of SARS-CoV-2 is a sub-optimal furin CS[11,18,19].

The furin cleavage site of SARS-CoV-2 spike protein promotes entry into epithelial cell lines and cultures but adversely affects entry into Vero and 293T cells.

To investigate a role for S1/S2 furin CS of SARS-CoV-2 in virus replication in different cell types, we performed competition assays, taking a mixed SARS-CoV-2 population containing 70% ΔCS mutant and 30% WT (as determined by deep sequencing of the S1/S2 CS; Figure 1e) inoculated onto Vero E6 cells, human intestinal Caco-2 cells or air-liquid interface, differentiated human airway

epithelial cell cultures (HAEs) at a low multiplicity of infection (MOI) enabling multicycle replication. By 72 hours, the ΔCS mutant outcompeted WT in Vero E6 cells, whereas WT became predominant in the Caco-2 cells. In primary HAE cultures, the WT rapidly outcompeted the ΔCS virus which was almost undetectable after 72 hours (Figure 1f). We also infected Calu-3 (human lung) cells with clonal WT or ΔCS virus at an MOI of 0.1 (Figure 1g). WT virus replicated robustly and reached peak titres greater than 10^5 pfu after 48 hours. Conversely, ΔCS virus was unable to productively infect Calu-3 cells and no infectious titre was detected at any time point.

Next, we probed the ability of PV with different mutant spike proteins to enter different human cell lines: 293T cells expressing human ACE2, Caco-2 cells or Calu-3 cells (Figure 2D-F). PV bearing the envelope of amphotropic murine leukaemia virus (MLV-A), Indiana vesicular stomatitis virus glycoprotein (VSV-G), or produced without any viral glycoproteins (bald) were used as positive and negative controls throughout. As in the Vero E6 cells (Figure 1e), a clear negative correlation was seen between efficiency of furin cleavage of the spike and entry in 293T-ACE2 cells (Figure 1h). PV with WT SARS-CoV-2 spike entered 293T-ACE2s less efficiently than SARS-CoV, while SARS-CoV-2 spike mutants without furin cleavage (monoCS/ΔCS/Δflank) entered cells significantly more efficiently (>3-fold compared to WT). Introduction of the optimised furin CS (H5CS) dramatically decreased entry (~10-fold lower than WT; $P < 0.001$). In Caco-2 and Calu-3 cells, the opposite trend was observed in accordance with the efficiency of virus replication in Caco-2, Calu-3 and primary HAE cells (Figure 1i,j). Mutants unable to be cleaved by furin, including ΔCS, entered cells significantly less efficiently than WT and H5CS (>2-fold lower in Caco-2 and ~5-fold lower in Calu-3 cells).

Entry of SARS-CoV-2 into 293T cells is dependent on cathepsins while entry into Caco-2, Calu-3 and primary HAE cells is dependent on TMPRSS2

As well as at the S1/S2 junction, coronavirus spike proteins require cleavage by host cell proteases at the S2' site to enable viral/host cell membrane fusion. To investigate whether the

different cell entry phenotypes seen in 293T-ACE2/Vero vs Caco-2/Calu-3/HAE cells were due to differences in protease usage, we performed PV entry assays in the presence of protease inhibitors: camostat, which inhibits serine proteases such as TMPRSS2, and E-64d, which inhibits cathepsins. Both drugs have been shown to be inhibitory to SARS-CoV and SARS-CoV-2 entry[32,33].

In 293T-ACE2 cells, camostat pre-treatment did not inhibit PV entry whereas E-64d did (Figure 2a). In Caco-2 cells, a different pattern was seen: camostat had a significant impact on PVs bearing spike proteins with furin CSs, whereas E-64d inhibited only PV with spikes which were not cleaved by furin (Figure 2b). In Calu-3 cells, camostat significantly inhibited entry of all coronavirus PVs while E-64d also had a modest, but significant ($P < 0.05$), effect on the ΔCS mutant (Figure 2c). Control PV expressing MLV-A or VSV-G, which are not reliant on cathepsins or serine proteases for entry[33], were not significantly affected by either drug in any cell line.

To confirm dependence of whole SARS-CoV-2 virus on serine proteases in primary airway cells, we examined multicycle replication of clonal WT and ΔCS viruses on HAE cells in the presence or absence of camostat (Figure 2d). Consistent with the results of the competition assay, the ΔCS virus grew to significantly lower titres than WT. Addition of 50 μM camostat severely delayed replication of WT virus and abrogated that of ΔCS, without any loss of HAE integrity, as measured by transepithelial electronic resistance (Figure 3d, Extended Data Figure 2a). Thus in HAEs, cleavage by serine proteases is required for efficient entry.

To investigate whether differences in endogenous levels of receptor or proteases accounted for different entry pathways for SARS-CoV-2 in different human cell types, we quantified expression of ACE2, TMPRSS2 and cathepsin mRNAs (Figure 2e-h). All three human cell lines and the primary HAE cultures expressed ACE2 and cathepsin L to varying degrees. However, 293T-ACE2 cells lacked any detectable TMPRSS2 expression, explaining why camostat had little effect in these cells. Previous studies have shown Vero E6 cells express no endogenous TMPRSS2[30,31].

Expression of TMPRSS2 promotes entry of SARS-CoV-2 with a polybasic cleavage site.

To investigate whether TMPRSS2 expression enhanced entry of viruses with furin cleavable spike proteins, we compared the entry of PVs transiently in 293T cells co-expressing ACE2 with or without TMPRSS2 (Figure 3a). TMPRSS2 promoted entry of all coronavirus PVs, even though TMPRSS2 expression led to lower levels of cell-associated ACE2 due to ACE2 being a substrate of TMPRSS2 (Extended Data Figure 2b)[34]. The TMPRSS2-mediated enhancement of PV entry was particularly potent for the PVs harbouring furin CS containing spike (>15-fold), compared to the non furin-cleaved mutants (<10-fold) indicating that expression of TMPRSS2 favours the entry into cells of PVs with furin CSs.

We further tested the ability of authentic WT and ΔCS SARS-CoV-2 to replicate in Vero E6 cells compared to Vero E6 cells constitutively expressing TMPRSS2[35,36]. In line with the previous competition assay (Figure 1e), clonal ΔCS replicated significantly more rapidly than WT in Vero E6 cells (Figure 3b). Conversely in Vero E6/TMPRSS2 cells, WT virus grew to significantly higher titres by 24 hours post-infection and both viruses reached similar peak titres at 48 hours post infection (Figure 3c). Overall, these data confirm that TMPRSS2 expression gives WT SARS-CoV-2 a replication advantage over viruses lacking the furin cleavage site.

The furin cleavage site of SARS-CoV-2 allows escape from endosomal IFITM proteins in TMPRSS2 expressing cells

TMPRSS2 cleavage has been proposed to allow other coronaviruses to avoid restriction by endosomal IFITM proteins, such as IFITM2/3[37,38]. Therefore, we hypothesised that the furin CS may enable SARS-CoV-2 also to avoid these IFITM proteins, known to restrict SARS-CoV and SARS-CoV-2 entry in the absence of TMPRSS2[38-40]. The antifungal agent amphotericin B (amphoB) is well described as inhibiting the restriction imposed by endosomal/endolysosomal IFITM proteins, potentially through modulating the host membrane fluidity [38,39,41]. All the human cells lines used herein, 293T-ACE2, Caco-2, Calu-3 and HAEs constitutively expressed all three antiviral IFITM

paralogues, even in the absence of exogenous interferon (Figure 2e-h). We pre-treated cells with amphoB and investigated the effect on PV entry. In 293T-ACE2 cells, entry of all coronavirus PV was improved by amphoB pre-treatment, showing that all PVs entered these cells through endosomes (Figure 3d). Conversely, in Caco-2 and Calu-3 cells, entry of PVs with uncleaved spikes was boosted by amphoB treatment, whereas there was little or no effect on the entry of PVs with furin CS containing spikes (Figure 3e,f).

Next, we co-expressed ACE2 and TMPRSS2 with or without IFITM3 in 293T cells. Entry of PVs with furin CS containing spikes were less inhibited by IFITM3 than those with spikes that could not be furin cleaved (Figure 3e, Extended Data Figure 2c).

Finally, we investigated the effect of amphoB treatment on SARS-CoV-2 replication in Calu-3 and HAEs. In both cell types amphoB had no effect on WT virus replication, but greatly increased the replication of the ΔCS mutant (Figure 3h,i). This implies that endosomal IFITM proteins are a major block for entry of viruses without furin CSs in TMPRSS2-expressing cells.

The SARS-CoV-2 polybasic cleavage site promotes replication in the respiratory tract and transmission in a ferret model

To investigate whether the furin CS plays a role in the transmission of SARS-CoV-2, we used ferrets as an *in vivo* model. Ferrets are commonly used in transmission studies of respiratory pathogens such as influenza and, more recently, SARS-CoV-2[42-44]. Furthermore, mink, which are closely related to ferrets, are highly susceptible to reverse zoonotic infection and outbreaks in mink farms show that SARS-CoV-2 is efficiently transmitted between these animals[45,46]. Four ferrets per group were each infected intranasally with 10^5 pfu of clonal WT or ΔCS mutant SARS-CoV-2. After 24 hours, naïve contact ferrets were co-housed with each donor. Ferrets were nasal washed daily for the following 2 weeks and virus shedding was titrated by qRT-PCR and by $TCID_{50}$ (Figure 4a,b, Extended Data Figure 3a,b). All eight directly inoculated ferrets shed virus robustly for 9-12 days (Figure 4a). The WT infected group shed more virus than ferrets infected with ΔCS virus, indicated by

higher infectious virus and E gene copy numbers, the latter significant at days 2-4. In the WT group, 2/4 contact ferrets became productively infected indicated by infectious virus, E gene loads, and seroconversion, whereas no transmission from donor ferret infected with ΔCS mutant virus was detected (Figure 4b, Extended Data Figures 3a-c). In nasal washes of the two remaining ferrets exposed to donors infected with WT virus, low E gene copy numbers were detected but no infectious virus was measured, and these animals remained seronegative at 14 days post exposure, implying these ferrets were not infected (Extended Data Figure 3c).

Next, a competition assay was performed whereby four ferrets were inoculated intra-nasally with 10^5 pfu of the previously described mixture of WT and ΔCS virus at a 30:70 ratio (Figure 4c,d). One day post-inoculation, naïve contact ferrets were co-housed with each donor animal and all animals were nasal washed daily. All directly inoculated ferrets became productively infected, shedding infectious virus and detectable E gene between days 1-12 (Figure 4c). Interestingly, which virus genotype became dominant in the nasal washes of the directly infected ferrets appeared to vary stochastically; in two animals the WT virus became predominant by day 2; these animals shed the highest levels of infectious virus and E gene RNA. In the remaining two directly inoculated animals, the ΔCS virus remained the majority species or outcompeted the WT over the course of the experiment. Productive transmission was only recorded in a single contact which was co-caged with one of the animals shedding predominantly WT virus (Figure 4d). The ΔCS genotype was detectable in this single contact at low levels on day 3, 8 and 9, but at all times the WT virus clearly predominated. This animal was the only contact ferret to seroconvert, confirming the other 3 contact ferrets were not productively infected (Extended Data Figure 4d). No ferrets from either experiment showed appreciable fever or weight loss (Extended Data Figures 4a-c, 3d,e). Together these results strongly suggest that the furin CS of SARS-CoV-2 spike is a determinant of transmission in the ferret model.

SARS-CoV-2 spike variants with deletions or mutations in the polybasic cleavage site are detectable in human tissues.

Finally, we investigated whether spike deletion mutants were present in human clinical samples and, if so, whether they were more likely to be found in a particular organ. Initially we downloaded 100,000 genome sequences from GISAID and found only 2 sequences from clinical swabs with CS deletions (Supplementary Table S1). Next, we deep sequenced the S1/S2 CS from 24 previously described samples taken from five different post-mortem cases, including tissues from the respiratory and gastrointestinal tract, the brain, heart, bone marrow, kidney, tongue and spleen[47]. Sequencing revealed very low levels of viral RNA bearing different S1/S2 CS deletion (<1%) from heart and spleen tissue from 2 separate patients (Supplementary Table S2). The three deletions reported in Supplementary Table S1 are not previously reported but are similar to those seen upon passage in Vero E6 cells. OS5 deletes 4 amino acids after the CS similar to a deletion reported in a recent study[27]; OS19-1 overlaps with most of Δflank and OS19-2 completely removes the S1/S2 site, similar to ΔCS. We have also observed identical deletions to OS19-2 upon passaging the clonal WT virus in Vero E6 cells. The S1/S2 cleavage site of SARS-CoV-2 lies on an exposed, flexible loop, therefore any deletion, whether directly of the polybasic site or the flanking region likely results in a reduced ability for furin cleave this region[13,48], as demonstrated throughout this study by the Δflank and ΔCS mutants showing identical phenotypes. These results are consistent with the conclusion that S1/S2 cleavage site deletions can arise *in vivo*, albeit at a very low rate.

Discussion

An insertion of 4 amino acids in the SARS-CoV-2 spike protein occurred during its emergence from an animal reservoir and created a suboptimal furin cleavage site (CS)[11]. Here, we propose a mechanism by which this conferred an advantage to the virus in the human airway enabling efficient human-to-human transmission. We confirm that pre-cleavage of the spike during viral egress enhances entry of progeny virions into TMPRSS2-expressing cells such as those abundant in

respiratory tissue[18,19]. TMPRSS2 cleaves spike at S2' and facilitates early entry at or near the cell surface, as opposed to late entry through the endosome. This allows virus to avoid the potent endosomal/endolysosomal restriction factors, the IFITM proteins, which inhibit viral membrane fusion. Indeed, Winstone *et al* recently showed IFITM2 can potently restrict entry of SARS-CoV-2 variants that lack the spike polybasic site, and that this restriction accounts for the majority of type I interferon-induced inhibition of SARS-CoV-2[49]. Viruses that lack a furin CS are forced to enter cells through the IFITM containing endosome where the spike can be cleaved at S1/S2 and S2' sites by cathepsins. However, furin cleaved spike is not always advantageous: in cell types like Vero, lacking TMPRSS2 expression, viruses without the furin CS gain an advantage, potentially because they are more stable, since spike cleavage may result in premature shedding of the S1 subunit altogether and abrogate receptor binding[50]. We show that, in contrast with WT SARS-CoV-2, a virus with a deleted furin CS did not replicate to high titres in the upper respiratory tract of ferrets and did not transmit to cohoused sentinel animals, in agreement with similar experiments using hamsters[28]. We have also found that furin CS deletions arise naturally at very low levels across different human organs during severe infection. Indeed, we note only 2 recorded genomes on GISAID out of 100,690 (as of 16/9/20) with furin CS deletions (Supplemental Table S1). Given the ease of loss of the furin CS in cell culture, the lack of these mutants in sequenced isolates is further evidence that the furin CS is essential for sustained transmission of SARS-CoV-2 in humans.

Our study confirms TMPRSS2 as a potential drug target. Whilst inhibition of TMPRSS2 protease activity would not prevent infection via the endosome, using this pathway is detrimental to virus replication in airway cells. We have shown in this study that the protease inhibitor, camostat, is highly efficient at blocking SARS-CoV-2 replication in human airway cells and we note that clinical trials are ongoing [ClinicalTrials.gov Identifier: NCT04455815]. Our study also confirms the limitations of relying on Vero E6 cells as a system for developing classes of drugs such as entry inhibitors as they do not accurately reflect the preferred entry mechanism of SARS-CoV-2 into human airway cells[51,52]. Indeed, the data here explains why chloroquine is ineffective in clinic against

SARS-CoV-2[51], since during replication in the human airway WT SARS-CoV-2 has evolved to enter cells without the need for endosomal acidification.

Presence of a furin CS at the S1/S2 junction is not uncommon in human coronaviruses; while half of human seasonal coronaviruses and MERS-CoV do, the remaining strains and SARS-CoV do not[6,16]. Thus, furin-mediated cleavage of spike is not an absolute requirement for efficient human respiratory transmission. Monitoring animal coronaviruses will likely be important in predicting and preventing future pandemics. We suggest that gain of a furin CS in the wider SARS-related coronaviruses is a cause for concern. The polybasic insertion to the S1/S2 CS provides a significant fitness advantage in TMPRSS2 expressing cells and is likely essential for efficient human transmission. We also note that the SARS-CoV-2 CS remains suboptimal for furin cleavage. It is unclear if this is a trade-off (i.e. with stability of spike) or whether further optimisation of this site could result in higher transmissibility. In this regard, multiple SARS-CoV-2 variants have recently emerged and spread rapidly including some, such as the B.1.1.7 'UK' variant, that have mutations proximal to the S1/S2 cleavage site predicted to enhance furin cleavage. This further emphasises the role of this site for virus transmission and the importance of continued monitoring as SARS-CoV-2 circulates in the human population[53].

References

1 Zhou, P. *et al.* A pneumonia outbreak associated with a new coronavirus of probable bat origin. *Nature* **579**, 270-273, doi:10.1038/s41586-020-2012-7 (2020).

2 Zhu, N. *et al.* A Novel Coronavirus from Patients with Pneumonia in China, 2019. *N Engl J Med* **382**, 727-733, doi:10.1056/NEJMoa2001017 (2020).

3 World Health Organisation. *WHO Coronavirus Disease (COVID-19) Dashboard*, <https://covid19.who.int/> (2021).

4 Matsuyama, S. *et al.* Efficient activation of the severe acute respiratory syndrome coronavirus spike protein by the transmembrane protease TMPRSS2. *J Virol* **84**, 12658-12664, doi:10.1128/JVI.01542-10 (2010).

5 Simmons, G. *et al.* Inhibitors of cathepsin L prevent severe acute respiratory syndrome coronavirus entry. *Proc Natl Acad Sci U S A* **102**, 11876-11881, doi:10.1073/pnas.0505577102 (2005).

6 Millet, J. K. & Whittaker, G. R. Host cell entry of Middle East respiratory syndrome coronavirus after two-step, furin-mediated activation of the spike protein. *Proc Natl Acad Sci U S A* **111**, 15214-15219, doi:10.1073/pnas.1407087111 (2014).

7 Belouzard, S., Chu, V. C. & Whittaker, G. R. Activation of the SARS coronavirus spike protein via sequential proteolytic cleavage at two distinct sites. *Proc Natl Acad Sci U S A* **106**, 5871-5876, doi:10.1073/pnas.0809524106 (2009).

8 Benton, D. J. *et al.* Receptor binding and priming of the spike protein of SARS-CoV-2 for membrane fusion. *Nature*, doi:10.1038/s41586-020-2772-0 (2020).

9 Madu, I. G., Roth, S. L., Belouzard, S. & Whittaker, G. R. Characterization of a highly conserved domain within the severe acute respiratory syndrome coronavirus spike protein S2 domain with characteristics of a viral fusion peptide. *J Virol* **83**, 7411-7421, doi:10.1128/JVI.00079-09 (2009).

10 Li, W. *et al.* Angiotensin-converting enzyme 2 is a functional receptor for the SARS coronavirus. *Nature* **426**, 450-454, doi:10.1038/nature02145 (2003).

11 Shang, J. *et al.* Cell entry mechanisms of SARS-CoV-2. *Proc Natl Acad Sci U S A*, doi:10.1073/pnas.2003138117 (2020).

12 Coutard, B. *et al.* The spike glycoprotein of the new coronavirus 2019-nCoV contains a furin-like cleavage site absent in CoV of the same clade. *Antiviral Res* **176**, 104742, doi:10.1016/j.antiviral.2020.104742 (2020).

13 Jaimes, J. A., Millet, J. K. & Whittaker, G. R. Proteolytic Cleavage of the SARS-CoV-2 Spike Protein and the Role of the Novel S1/S2 Site. *iScience* **23**, 101212, doi:10.1016/j.isci.2020.101212 (2020).

14 Andersen, K. G., Rambaut, A., Lipkin, W. I., Holmes, E. C. & Garry, R. F. The proximal origin of SARS-CoV-2. *Nat Med* **26**, 450-452, doi:10.1038/s41591-020-0820-9 (2020).

15 Boni, M. F. *et al.* Evolutionary origins of the SARS-CoV-2 sarbecovirus lineage responsible for the COVID-19 pandemic. *Nat Microbiol*, doi:10.1038/s41564-020-0771-4 (2020).

16 Le Coupanec, A. *et al.* Cleavage of a Neuroinvasive Human Respiratory Virus Spike Glycoprotein by Proprotein Convertases Modulates Neurovirulence and Virus Spread within the Central Nervous System. *PLoS Pathog* **11**, e1005261, doi:10.1371/journal.ppat.1005261 (2015).

17 Park, J. E. *et al.* Proteolytic processing of Middle East respiratory syndrome coronavirus spikes expands virus tropism. *Proc Natl Acad Sci U S A* **113**, 12262-12267, doi:10.1073/pnas.1608147113 (2016).

18 Hoffmann, M., Kleine-Weber, H. & Pohlmann, S. A Multibasic Cleavage Site in the Spike Protein of SARS-CoV-2 Is Essential for Infection of Human Lung Cells. *Mol Cell*, doi:10.1016/j.molcel.2020.04.022 (2020).

19 Bestle, D. *et al.* TMPRSS2 and furin are both essential for proteolytic activation of SARS-CoV-2 in human airway cells. *Life Sci Alliance* **3**, doi:10.26508/lsa.202000786 (2020).

20 Johnson, B. A. *et al.* Loss of furin cleavage site attenuates SARS-CoV-2 pathogenesis. *Nature*, doi:10.1038/s41586-021-03237-4 (2021).

21 Lau, S. Y. *et al.* Attenuated SARS-CoV-2 variants with deletions at the S1/S2 junction. *Emerg Microbes Infect* **9**, 837-842, doi:10.1080/22221751.2020.1756700 (2020).

22 Liu, Z. *et al.* Identification of common deletions in the spike protein of SARS-CoV-2. *J Virol*, doi:10.1128/JVI.00790-20 (2020).

23 Ogando, N. S. *et al.* SARS-coronavirus-2 replication in Vero E6 cells: replication kinetics, rapid adaptation and cytopathology. *J Gen Virol*, doi:10.1099/jgv.0.001453 (2020).

24 Wong, Y. C. *et al.* Natural transmission of bat-like SARS-CoV-2PRRA variants in COVID-19 patients. *Clin Infect Dis*, doi:10.1093/cid/ciaa953 (2020).

25 Klimstra, W. B. *et al.* SARS-CoV-2 growth, furin-cleavage-site adaptation and neutralization using serum from acutely infected hospitalized COVID-19 patients. *J Gen Virol*, doi:10.1099/jgv.0.001481 (2020).

26 Davidson, A. D. *et al.* Characterisation of the transcriptome and proteome of SARS-CoV-2 reveals a cell passage induced in-frame deletion of the furin-like cleavage site from the spike glycoprotein. *Genome Med* **12**, 68, doi:10.1186/s13073-020-00763-0 (2020).

27 Sasaki, M. *et al.* SARS-CoV-2 variants with mutations at the S1/S2 cleavage site are generated in vitro during propagation in TMPRSS2-deficient cells. *PLoS Pathog* **17**, e1009233, doi:10.1371/journal.ppat.1009233 (2021).

28 Zhu, Y. *et al.* A genome-wide CRISPR screen identifies host factors that regulate SARS-CoV-2 entry. *Nat Commun* **12**, 961, doi:10.1038/s41467-021-21213-4 (2021).

29 Xia, S. *et al.* The role of furin cleavage site in SARS-CoV-2 spike protein-mediated membrane fusion in the presence or absence of trypsin. *Signal Transduct Target Ther* **5**, 92, doi:10.1038/s41392-020-0184-0 (2020).

30 Shirato, K., Kawase, M. & Matsuyama, S. Middle East respiratory syndrome coronavirus infection mediated by the transmembrane serine protease TMPRSS2. *J Virol* **87**, 12552-12561, doi:10.1128/JVI.01890-13 (2013).

31 Bertram, S. *et al.* TMPRSS2 and TMPRSS4 facilitate trypsin-independent spread of influenza virus in Caco-2 cells. *J Virol* **84**, 10016-10025, doi:10.1128/JVI.00239-10 (2010).

32 Ou, X. *et al.* Characterization of spike glycoprotein of SARS-CoV-2 on virus entry and its immune cross-reactivity with SARS-CoV. *Nat Commun* **11**, 1620, doi:10.1038/s41467-020-15562-9 (2020).

33 Hoffmann, M. *et al.* SARS-CoV-2 Cell Entry Depends on ACE2 and TMPRSS2 and Is Blocked by a Clinically Proven Protease Inhibitor. *Cell* **181**, 271-280 e278, doi:10.1016/j.cell.2020.02.052 (2020).

34 Shulla, A. *et al.* A transmembrane serine protease is linked to the severe acute respiratory syndrome coronavirus receptor and activates virus entry. *J Virol* **85**, 873-882, doi:10.1128/JVI.02062-10 (2011).

35 Matsuyama, S. *et al.* Enhanced isolation of SARS-CoV-2 by TMPRSS2-expressing cells. *Proc Natl Acad Sci U S A* **117**, 7001-7003, doi:10.1073/pnas.2002589117 (2020).

36 Nao, N. *et al.* Consensus and variations in cell line specificity among human metapneumovirus strains. *PLoS One* **14**, e0215822, doi:10.1371/journal.pone.0215822 (2019).

37 Bertram, S. *et al.* TMPRSS2 activates the human coronavirus 229E for cathepsin-independent host cell entry and is expressed in viral target cells in the respiratory epithelium. *J Virol* **87**, 6150-6160, doi:10.1128/JVI.03372-12 (2013).

38 Zheng, M. *et al.* Bat SARS-Like WIV1 coronavirus uses the ACE2 of multiple animal species as receptor and evades IFITM3 restriction via TMPRSS2 activation of membrane fusion. *Emerg Microbes Infect* **9**, 1567-1579, doi:10.1080/22221751.2020.1787797 (2020).

39 Zhao, X. *et al.* LY6E Restricts the Entry of Human Coronaviruses, Including the Currently Pandemic SARS-CoV-2. *J Virol*, doi:10.1128/JVI.00562-20 (2020).

40 Huang, I. C. *et al.* Distinct patterns of IFITM-mediated restriction of filoviruses, SARS coronavirus, and influenza A virus. *PLoS Pathog* **7**, e1001258, doi:10.1371/journal.ppat.1001258 (2011).

41 Lin, T. Y. *et al.* Amphotericin B increases influenza A virus infection by preventing IFITM3-mediated restriction. *Cell Rep* **5**, 895-908, doi:10.1016/j.celrep.2013.10.033 (2013).

42 Kim, Y. I. *et al.* Infection and Rapid Transmission of SARS-CoV-2 in Ferrets. *Cell Host Microbe* **27**, 704-709 e702, doi:10.1016/j.chom.2020.03.023 (2020).

43 Richard, M. *et al.* SARS-CoV-2 is transmitted via contact and via the air between ferrets. *Nat Commun* **11**, 3496, doi:10.1038/s41467-020-17367-2 (2020).

44 Belser, J. A. *et al.* Ferrets as Models for Influenza Virus Transmission Studies and Pandemic Risk Assessments. *Emerg Infect Dis* **24**, 965-971, doi:10.3201/eid2406.172114 (2018).

45 Enserink, M. Coronavirus rips through Dutch mink farms, triggering culls. *Science* **368**, 1169, doi:10.1126/science.368.6496.1169 (2020).

46 Oude Munnink, B. B. *et al.* Transmission of SARS-CoV-2 on mink farms between humans and mink and back to humans. *Science*, doi:10.1126/science.abe5901 (2020).

47 Hanley, B. *et al.* Histopathological findings and viral tropism in UK patients with severe fatal COVID-19: a post-mortem study. *Lancet Microbe*, doi:10.1016/S2666-5247(20)30115-4 (2020).

48 Lemmin, T., Kalbermatter, D., Harder, D., Plattet, P. & Fotiadis, D. Structures and dynamics of the novel S1/S2 protease cleavage site loop of the SARS-CoV-2 spike glycoprotein. *Journal of Structural Biology: X* **4**, 100038, doi:https://doi.org/10.1016/j.yjsbx.2020.100038 (2020).

49 Winstone, H. *et al.* The polybasic cleavage site in the SARS-CoV-2 spike modulates viral sensitivity to Type I interferon and IFITM2. *J Virol*, doi:10.1128/JVI.02422-20 (2021).

50 Zhang, L. *et al.* SARS-CoV-2 spike-protein D614G mutation increases virion spike density and infectivity. *Nat Commun* **11**, 6013, doi:10.1038/s41467-020-19808-4 (2020).

51 Hoffmann, M. *et al.* Chloroquine does not inhibit infection of human lung cells with SARS-CoV-2. *Nature*, doi:10.1038/s41586-020-2575-3 (2020).

52 Ou, T. *et al.* Hydroxychloroquine-mediated inhibition of SARS-CoV-2 entry is attenuated by TMPRSS2. *PLoS Pathog* **17**, e1009212, doi:10.1371/journal.ppat.1009212 (2021).

53 Rambaut, A. *et al.* Preliminary genomic characterisation of an emergent SARS-CoV-2 lineage in the UK defined by a novel set of spike mutations. (virological.org, 2020).

54 Kärber, G. Beitrag zur kollektiven Behandlung pharmakologischer Reihenversuche. *Naunyn-Schmiedebergs Archiv für experimentelle Pathologie und Pharmakologie* **162**, 480-483, doi:10.1007/BF01863914 (1931).

55 Long, J., Wright, E., Molesti, E., Temperton, N. & Barclay, W. Antiviral therapies against Ebola and other emerging viral diseases using existing medicines that block virus entry. *F1000Res* **4**, 30, doi:10.12688/f1000research.6085.2 (2015).

56 McKay, P. F. *et al.* Self-amplifying RNA SARS-CoV-2 lipid nanoparticle vaccine candidate induces high neutralizing antibody titers in mice. *Nat Commun* **11**, 3523, doi:10.1038/s41467-020-17409-9 (2020).

57 Rebendenne, A. *et al.* SARS-CoV-2 triggers an MDA-5-dependent interferon response which is unable to control replication in lung epithelial cells. *Journal of Virology*, JVI.02415-02420, doi:10.1128/jvi.02415-20 (2021).

58 Edie, S. *et al.* Survey of Human Chromosome 21 Gene Expression Effects on Early Development in Danio rerio. *G3 (Bethesda)* **8**, 2215-2223, doi:10.1534/g3.118.200144 (2018).

59 Sumner, R. P. *et al.* Disrupting HIV-1 capsid formation causes cGAS sensing of viral DNA. *EMBO J*, e103958, doi:10.15252/embj.2019103958 (2020).

60 Goldhill, D. H. *et al.* Determining the Mutation Bias of Favipiravir in Influenza Virus Using Next-Generation Sequencing. *J Virol* **93**, doi:10.1128/JVI.01217-18 (2019).

61 Goldhill, D. H. *et al.* The mechanism of resistance to favipiravir in influenza. *Proc Natl Acad Sci U S A* **115**, 11613-11618, doi:10.1073/pnas.1811345115 (2018).

62 Jabara, C. B., Jones, C. D., Roach, J., Anderson, J. A. & Swanstrom, R. Accurate sampling and deep sequencing of the HIV-1 protease gene using a Primer ID. *Proc Natl Acad Sci U S A* **108**, 20166-20171, doi:10.1073/pnas.1110064108 (2011).

63 Ma, D. *et al.* Expression of SARS-CoV-2 receptor ACE2 and TMPRSS2 in human primary conjunctival and pterygium cell lines and in mouse cornea. *Eye (Lond)* **34**, 1212-1219, doi:10.1038/s41433-020-0939-4 (2020).

64 Xu, Q. F. *et al.* Ultraviolet A Enhances Cathepsin L Expression and Activity via JNK Pathway in Human Dermal Fibroblasts. *Chin Med J (Engl)* **129**, 2853-2860, doi:10.4103/0366-6999.194654 (2016).

65 Zhou, Z. *et al.* The cAMP-responsive element binding protein (CREB) transcription factor regulates furin expression during human trophoblast syncytialization. *Placenta* **35**, 907-918, doi:10.1016/j.placenta.2014.07.017 (2014).

66 Xu-yang, Z. *et al.* Interferon-Induced Transmembrane Protein 3 Inhibits Hantaan Virus Infection, and Its Single Nucleotide Polymorphism rs12252 Influences the Severity of Hemorrhagic Fever with Renal Syndrome. *Frontiers in Immunology* **7**, doi:10.3389/fimmu.2016.00535 (2017).
67 Li, H. *et al.* Internal genes of a highly pathogenic H5N1 influenza virus determine high viral replication in myeloid cells and severe outcome of infection in mice. *PLoS Pathog* **14**, e1006821, doi:10.1371/journal.ppat.1006821 (2018).

Acknowledgments

SARS-CoV-2 virus was initially provided by Public Health England and we would like to thank Maria Zambon, Robin Gopal and Monika Patel for their help. This work was supported by BBSRC grants BB/R013071/1 (TPP, WB); BB/R007292/1 (LB, WB); BB/S008292/1 (JB, WB); BB/M02542X/1 (ADD, DAM) and Wellcome Trust grants 205100 (DHG, RYSD, WB); 200187 (JZ, RF, WB). This work was also supported by MRC grant MR/R020566/1 (MKW, ADD) and US FDA grant HHSF223201510104C (ADD, DAM). Additional support was provided from a grant from the King's College London King's Together Programme and the King's College London BHF Centre of Research Excellence grant RE/18/2/34213 to MG. OCS was supported by a Wellcome Trust studentship, RK was supported by Wellcome fellowship 216353/Z/19/Z, RP was supported by an MRC DTP studentship, JAH was supported by a BBSRC DTP studentship and ES was supported by an Imperial College President's Scholarship.

Author contributions statement

TPP, DHG, ADD, DAM and WSB conceived and planned experiments. TPP, DHG, JZ, LB, RF, OCS, RK, RP, JCB, RYSD, LB, MKW, JAH and ES performed the experiments. LB, OCS, RP, BH and MO processed the autopsy samples. MO, MG, ADD, DAM and WSB provided supervision. TPP, DHG and WB wrote the manuscript with input from all other authors.

Competing interests statement

The authors declare they have no competing interests.

Methods

Biosafety and ethics statement

All work performed was approved by the local genetic manipulation (GM) safety committee of Imperial College London, St. Mary's Campus (centre number GM77), and the Health and Safety Executive of the United Kingdom, under reference CBA1.77.20.1. Animal research was carried out under a United Kingdom Home Office License, P48DAD9B4.

Human samples used in this research project were obtained from the Imperial College Healthcare Tissue Bank (ICHTB). ICHTB is supported by the NIHR Biomedical Research Centre based at Imperial College Healthcare NHS Trust and Imperial College London. ICHTB is approved by Wales REC3 to release human material for research (17/WA/0161), and the samples for this project (R20012) were issued from subcollection reference number MED_MO_20_011.

Cells and viruses

African green monkey kidney cells (Vero E6; ATCC® CRL-1586) and human embryonic kidney cells (293T; ATCC® CRL-11268) were maintained in Dulbecco's modified Eagle's medium (DMEM), 10% fetal calf serum (FCS), 1% non-essential amino acids (NEAA), 1% penicillin-streptomycin (P/S). Human epithelial colorectal adenocarcinoma cells (Caco-2; ATCC® HTB-37) and human lung cancer cells (Calu-3; ATCC® HTB-55) were maintained in DMEM, 20% FCS, 1% NEAA, 1% P/S. VeroE6/TMPRSS2 cells were obtained from the Centre for AIDS Reagents (National Institute for Biological Standards and Control; 100978)[35,36], and maintained in DMEM, 10% FCS, 1% NEAA, 1% P/S, 1 mg/ml Geneticin (G418). Air liquid interface Human airway epithelial cells (HAEs) were purchased from Epithelix and maintained in Mucilair cell culture medium (Epithelix). All cell lines were maintained at 37^{o}C, 5% CO_2. HAE integrity in the presence of drugs was measured by transepithelial electrical resistance. Cell lines were not tested for mycoplasma contamination.

293T-hACE2 were generated by transducing 293Ts with an ACE2 expressing lentiviral vector, MT126, and selecting with 2 μg/ml puromycin, after selection cells were subsequently maintained with 1 μg/ml of puromycin.

The mixed SARS-CoV-2 WT/deletion virus mix was produced as previously described[26]. Briefly, the mix was generated by passaging the strain England/2/2020 (VE6-T), isolated by Public Health England (PHE), in Vero E6 cells whereby the deletion spontaneously arose[26]. The WT SARS-CoV-2 strain SARS-CoV-2 strain England/2/2020 (VE6-T) and the ΔCS mutant present in the original mixed stock were purified by serially diluting the stock (10-fold dilutions) in MEM supplemented with 2% FCS and adding the dilutions to either Vero E6 or Caco-2 cells in a 96 well plate. After 5 days incubation at 37 °C in 5% CO2, the culture supernatants in wells showing CPE at the highest dilution were again diluted and passaged on the same cells. After a further 5 days incubation, a 20 μl aliquot of culture supernatant from wells showing CPE at the highest dilution were used for RNA extraction and RT-PCR using a primer set designed to discriminate the WT and ΔCS mutant viruses. Culture supernatants containing either the WT or ΔCS mutant virus, with no sign of a mixed virus population were used to produce large scale stocks in Vero E6 cells. The presence of the expected virus in the stocks was verified by direct RNA sequencing using an Oxford Nanopore flow cell as previously described[26]. Clonally pure viruses were then further amplified by one additional passage in Vero E6/TMPRSS2 cells to make the working stocks of the viruses used throughout this study.

For plaque assays Vero E6 cells were used at 70-80% confluence. Cells were washed with PBS then serial dilutions of inoculum, diluted in serum-free DMEM, 1% NEAA, 1% P/S, were overlayed onto cells for one hour at 37^{o}C. Inoculum was then removed and replaced with SARS-CoV-2 overlay media (1x minimal essential media [MEM], 0.2% w/v bovine serum albumin, 0.16% w/v $NaHCO_3$, 10mM HEPES, 2mM L-Glutamine, 1x P/S, 0.6% w/v agarose). Plates were incubated for 3 days at 37^{o}C before overlay was removed and cells were stained for 1 hour at RT in crystal violet solution.

To titrate virus by $TCID_{50}$ Vero E6 cells were used at 70-80% confluence. Serial dilutions of virus, diluted in serum-free DMEM, 1% NEAA, 1% P/S, were added to each well and cells were left for 5 days before they were fixed with 2x crystal violet solution and analysed. 4 replicates of each sample were performed in tandem. $TCID_{50}$ titres were determined by the Spearman-Kärbar method[54].

Plasmids and cloning

Lentiviral packaging constructs pCSLW and pCAGGs-GAGPOL were made as previously described [55]. The codon-optimised spike proteins of SARS-CoV-2, SARS-CoV and MERS-CoV were a kind gift from Dr Paul McKay, Imperial College London[56]. Mutant SARS-CoV-2 expression plasmids were generated by site-directed mutagenesis. The lentiviral expression vector for human ACE2, MT126, was a kind gift from Dr Caroline Goujon, University of Montpellier[57]. ACE was further cloned into pCAGGs with the addition of a C-terminal FLAG-tag. TMPRSS2 expression plasmid was a kind gift from Roger Reeves (Addgene plasmid #53887 ; http://n2t.net/addgene:53887 ; RRID:Addgene_53887,[58]).

Syncytia formation assay

Vero E6 cells were seeded in 96-well plates ($6.5x10^3$ cells per well) to reach 70-80% confluency on the subsequent day. Transfection was performed using 100 ng of expression plasmid using 0.3 µl of FuGENE HD Transfection Reagent (Promega E2311) in 20 µl of Opti-MEM medium (Life Technologies). At 48 hr after drug treatment, plates were washed in 100 µL/well of 1 x PBS and fixed in 40 µl 4% PFA for 10 min at RT. After fixation cells were permeabilized in 0.1% Triton X-100 for 10 min at RT. Nuclei were stained using Hoechst 33342 (H3570 ThermoFisher), according to the manufacturer's instructions.

Image acquisition was performed using the Operetta CLS high content screening microscope (Perkin Elmer) with a Zeiss 20x (NA=0.80) objective. A total of 25 fields per well were imaged for the Hoechst 33342 channel (Excitation (Ex) 365-385nm, Emission (Em) 430-500nm). Images were

subsequently analysed, using the Harmony software (PerkinElmer). Images were first flatfield-corrected and nuclei were segmented using the "Find Nuclei" analysis module (Harmony). The thresholds for image segmentation were adjusted according to the signal-to-background ratio. Splitting coefficient was set in order to avoid splitting of overlapping nuclei (fused cells). All the cells that had a nuclear area greater than 3 times the average area of a single nucleus were considered as fused. Data were expressed as a percentage of fused cells by calculating the average number of fused cells normalized on the total number of cells per well.

Lentiviral pseudotype assays

Lentiviral pseudotypes (PV) were generated as previously described[55,59]. Briefly, 10cm^2 dishes of 293T cells were co-transfected with a mixture of 1 µg of the HIV packaging plasmid pCAGGs-GAGPOL, 1.5 µg of the luciferase reporter construct, pCSLW and 1 µg of each envelope protein in pcDNA3.1. PV containing supernatants were harvested at 48- and 72-hours post-transfection, passed through a 0.45 µm filter, aliquoted and frozen at -80^{o}C. Concentrated PV were produced by ultracentrifugation at 100,000 x g for 2 hours over a 20% sucrose cushion.

Cells were transduced by PV for 48 hours before lysis with cell culture lysis buffer (Promega). Luciferase luminescence was read on a FLUOstar Omega plate reader (BMF Labtech) using the Luciferase Assay System (Promega). The cathepsin inhibitor E-64d (Sigma-Aldrich), the serine protease inhibitor camostat mesylate (Abcam), or the antifungal and IFITM3 inhibitor Amphotericin B (Sigma-Aldrich) was pre-applied to cells for 1 hour at a concentration of 50 µM before addition of PV.

Overexpression experiments in 293T cells were performed by co-transfecting pCAGGS-ACE2-FLAG (1 µg) with TMPRSS2 (4 µg) or pCAGGs-IFITM3 (2.5ug) into 10 cm^2 dishes of 293Ts. Controls were transfected with equal amounts of empty vector instead of the named plasmid. After 24 hours, cells were washed, resuspended into fresh media and added to PV, or spun down for analysis by western blot.

Deep sequencing using primer ID

RNA was extracted from ferret nasal washes or cell supernatants using the QIAamp Viral RNA Mini Kit (Qiagen) with carrier RNA. RNA was reverse transcribed using Superscript IV (Invitrogen) and a barcoded primer for Primer ID (TGCGTTGATACCACTGCTTTNNNNANNNNANNNNAACTGAATTTTCTGCACCAAG). Primer ID attaches a unique barcode to each cDNA molecule during reverse transcription and allows for PCR and sequencing error correction[60-62]. PCR was performed using KOD polymerase (Merck) and the following primers (CAACTTACTCCTACTTGGCGT and XXXXTGCGTTGATACCACTGCTTT) giving a 272bp amplicon. XXXX was a 4-base barcode (CACA, GTTG, AGGA or TCTC) to allow for additional multiplexing. Samples were pooled and prepared for sequencing using NebNext Ultra II (NEB), then sequenced on an Illumina MiSeq with 300bp paired-end reads. Sequences were analysed in Geneious (v11) and a pipeline in R. Forward and reverse reads were paired using FLASh (https://ccb.jhu.edu/software/FLASH) before being mapped to a reference sequence and consensus sequences made for each barcode. A minimum cut-off of 3 reads per barcode was chosen. Raw sequences were deposited at www.ebi.ac.uk/ena, project number PRJEB40394. The analysis pipeline can be found at github.com/Flu1/Corona.

Deep sequencing from post-mortem samples

RNA from human post-mortem tissues from SARS-CoV-2 patients where COVID-19 was listed clinically as the cause of death were sourced and processed as previously described[47]. Briefly, fresh tissue was processed within biosafety level 3 facilities and total RNA was extracted using TRIzol (Invitrogen)-chloroform extraction followed by precipitation and purification using an RNeasy mini kit (Qiagen). RNA was reverse transcribed using Superscript IV (Invitrogen) and the following primer (GTCTTGGTCATAGACACTGGTAG). PCR was performed using KOD polymerase (Merck) and the following primers (GTCTTGGTCATAGACACTGGTAG and GGCTGTTTAATAGGGGCTGAAC) giving a 260bp amplicon. Samples were prepared for sequencing using NebNext Ultra II (NEB), then

sequenced on an Illumina MiSeq with 300bp paired-end reads. Sequences were analysed in Geneious (v11) and a pipeline in R. Forward and reverse reads were paired using FLASh (https://ccb.jhu.edu/software/FLASH) before being mapped to a reference sequence. Raw sequences were deposited at www.ebi.ac.uk/ena, project number PRJEB40394. The analysis pipeline can be found at github.com/Flu1/Corona.

Human Clinical Samples

A total of 100,690 SARS-CoV-2 genomes were downloaded from GISAID on 16/9/2020 and aligned to 234bp from the spike protein using Geneious. In frame deletions were identified in R and analysed to ensure that samples had not been passaged prior to sequencing. Code for this analysis can be found at github.com/Flu1/Corona.

Ferret transmission studies

Ferret (*Mustela putorius furo*) transmission studies were performed in a containment level 3 laboratory, using a bespoke isolator system (Bell Isolation Systems, U.K). Outbred female ferrets (16-20 weeks old), weighing 750-1000 g were used.

Prior to the study, ferrets were confirmed to be seronegative against SARS-CoV-2. Four donor ferrets were inoculated intranasally with 200 µl of 10^5 pfu of virus mix while lightly anaesthetised with ketamine (22 mg/kg) and xylazine (0.9 mg/kg). To assess direct contact transmission one naïve direct contact ferrets were introduced into each cage 1-day post initial inoculation.

All animals were nasal washed daily, while conscious, by instilling 2 mL of PBS into the nostrils, the expectorate was collected into disposable 250 ml sample pots. Ferrets were weighed daily post-infection, and body temperature was measured daily via subcutaneous IPTT-300 transponder (Plexx B.V, Netherlands).

Virus Neutralisation assay

The ability of ferret sera to neutralise wild type SARS-CoV-2 virus was assessed by neutralisation assay on Vero E6 cells. Heat-inactivated sera were serially diluted in assay diluent consisting of DMEM (Gibco, Thermo Fisher Scientific) with 1% penicillin-streptomycin (Thermo Fisher Scientific), 0.3% BSA fraction V (Thermo Fisher Scientific). Serum dilutions were incubated with 100 $TCID_{50}$/well of virus in assay diluent for 1 h at RT and transferred to 96-well plates pre-seeded with Vero E6 cells. Serum dilutions were performed in duplicate. Plates were incubated at 37°C, 5% CO2 for 5 days before adding an equal volume of 2X crystal violet stain to wells for 1 h. Plates were washed, wells were scored for cytopathic effect and a neutralisation titre calculated as the reciprocal of the highest serum dilution at which full virus neutralisation occurred.

qPCR

Viral RNA was extracted from Ferret nasal washes using the Qiagen Viral RNA mini kit, according to manufacturer's instructions.

Quantitative real-time RT-PCR (qRT-PCR) was performed using 7500 Real Time PCR system (ABI) in 20 µl reactions using AgPath-ID One-Step RT-PCR Reagents 10 µl RT-PCR buffer (2X) (Thermo Fisher), 5µl of RNA, 1 µl forward (5' ACAGGTACGTTAATAGTTAATAGCGT 3') and reverse primers (5' ATATTGCAGCAGTACGCACACA 3') and 0.5 µl probe (5' FAM-ACACTAGCCATCCTTACTGCGCTTCG -BBQ 3'). The following conditions were used: 45°C for 10 min, 1 cycle; 95°C for 15 min, 1 cycle; 95°C for 15 sec then 58°C for 30 sec, 45 cycles. For each sample, the C_t value for the target E gene was determined. Based on the standard curves, absolute E gene copy numbers were calculated.

RNA was extracted from cells using RNA extraction kits (QIAGEN, RNeasy Mini Kit, cat. 74106) following the manufacturer's instructions. Complementary DNA (cDNA) was synthesized in a reverse transcription step using Oligo-dT (RevertAid First Strand cDNA Synthesis, ThermoScientific, cat: K1621). To quantify mRNA levels, real-time quantitative PCR analysis with a gene specific primer

pair using SYBR green PCR mix (Applied Biosystems, cat: 4385612) was performed and data was analysed on the Applied Biosystems ViiATM 7 Real-Time PCR System. Primers were used as described elsewhere[63-67], and can be found in supplementary Table S3.

Western Blotting

To investigate cleavage of spike protein 293T cells transfected with 2.5 µg of spike expression plasmids (or empty vector). After 48 hours cells were lysed in RIPA buffer (150mM NaCl, 1% NP-40, 0.5% sodium deoxycholate, 0.1% SDS, 50mM TRIS, pH 7.4) supplemented with an EDTA-free protease inhibitor cocktail tablet (Roche). Cell lysates were then mixed with 4x Laemmli sample buffer (Bio-Rad) with 10% β-mercaptoethanol. Concentrated PV as described above were also diluted in Laemmli buffer.

Membranes were probed with mouse anti-FLAG (diluted 1/2000; F1804, Sigma), mouse anti-tubulin (diluted 1/5000; abcam; ab7291), mouse anti-p24 (diluted 1/2000; abcam; ab9071), rabbit anti-TMPRSS2 (diluted 1/2000; abcam; ab92323), rabbit anti-Fragilis/IFITM3 (diluted 1/2000; abcam; ab109429), rabbit anti-SARS spike protein (diluted 1/2000; NOVUS; NB100-56578) or rabbit anti-SARS-CoV-2 nucleocapsid (diluted 1/3000; SinoBiological; 40143-R019). Near infra-red (NIR) secondary antibodies, IRDye® 680RD Goat anti-mouse (diluted 1/10,000; abcam; ab216776), IRDye® 680RD Goat anti-rabbit (diluted 1/10,000; abcam; ab216777), IRDye® 800CW Goat anti-mouse (diluted 1/10,000; abcam; ab216772), or IRDye® 800CW Goat anti-rabbit (diluted 1/10,000; abcam; ab216773)) were subsequently used. Western blots were visualised using an Odyssey Imaging System (LI-COR Biosciences).

Data availability statement

The data that support the findings of this study are available from the corresponding author upon reasonable request. Raw sequences were deposited at www.ebi.ac.uk/ena, project number PRJEB40394. The analysis pipeline can be found at github.com/Flu1/Corona.

Code availability statement

All code is available at www.github.com/Flu1/corona.

Statistics and reproducibility

Statistics throughout this study were performed using One Way ANOVA or Student t-test and are described in the figure legends. No statistical method was used to predetermine sample size. 2 post-mortem samples were excluded from the analysis as they had low number of reads similar to the negative control sample and therefore were likely contamination. The experiments were not randomised, and the investigators were not blinded to allocation during experiments and outcome assessment.

Figure legends

Figure 1. The suboptimal furin cleavage site of SARS-CoV-2 spike enhances entry into mucosal epithelial and primary human airway cells.

(a) Amino acid sequence alignment of coronavirus furin cleavage site mutants used in this study. Mutants with potential S1/S2 furin cleavage sites shown in shades of orange while mutants without furin cleavage sites shown in shades of blue.
(b) Syncytia formation due to overexpression of different coronavirus spike proteins in Vero E6 cells. Percentage indicates proportion of nuclei in each field which have formed clear syncytia. Data plotted as mean + SD of 3 independent repeats. Statistical significance determined by one-way ANOVA with multiple comparisons against SARS-CoV-2 WT. **** indicates P value < 0.0001. Extended figure of representative fields shown in Extended Figure 1.
(c) Western blot analysis of concentrated lentiviral pseudotypes with different coronavirus spike proteins. Levels of lentiviral p24 antigen shown as loading control. Representative blot shown from N=3 independent repeats.
(d) Western blot analysis of concentrated WT and ΔCS SARS-CoV-2 viruses. Levels of nucleocapsid (N) protein shown as loading control. Representative blot shown from N=2 independent repeats.
(e) SARS-CoV-2 competition assay growth curve between WT and ΔCS virus in Vero E6 and Caco-2 cells. Cells infected at an MOI of 0.1. Starting inoculum ratio shown on the left-hand bar while proportions of virus as determined by deep sequencing at 72 hours post-inoculation shown on the right. Virus titres determined by plaque assay at 72 hours post-inoculation shown in superimposed white data points. All results indicate triplicate repeats plotted as mean + SD.
(f) SARS-CoV-2 competition assay growth curve between WT and ΔCS virus in human airway epithelial cells (HAEs). Cells infected at an MOI of 0.1. Starting inoculum ratio shown at time 0, proportions of virus determined by deep sequencing. All time points taken from triplicate repeats. Virus replication determined by plaque assay and shown as imposed white data points. Data plotted as mean + SD.
(g) Head-to-head replication kinetics of clonal WT and ΔCS viruses in Calu-3 human lung cells. Cells infected at an MOI of 0.1. All time points taken from triplicate repeats plotted as mean + SD. Data shown is representative replicate from (total N=2) repeats. Virus replication determined by plaque assay.
(h,i,j) Entry of lentiviral pseudotypes (PV) containing different viral glycoproteins into 293T-ACE2 (h), Caco-2 (i) and Calu-3 (j) cells. Cells transduced with different PV and lysed 48 hours later and analysed by firefly luciferase luminescence. Data shown as raw luminescence units. All assays performed in sextuplicate (Coronavirus pseudovirus) or triplicate (non-coronavirus controls) and plotted as mean + SD. Data shown is representative replicate from (N=4) independent repeats. Statistics determined by one-way ANOVA on Log-transformed data (after determining log normality by the Shapiro-Wilk test and QQ plot.) *, $0.05 \geq P > 0.01$; **, $0.01 \geq P > 0.001$; ***, $0.001 \geq P > 0.0001$; ****, $P \leq 0.0001$.

Figure 2. The furin cleavage site of SARS-CoV-2 spike allows more efficient serine-protease dependent entry into airway cells.

(a,b,c) Inhibition of entry of lentiviral pseudotypes into (a) 293T-ACE2, (b) Caco-2 or (c) Calu-3 cells by the serine protease inhibitor, camostat (green bars) or the cathepsin inhibitor, E64-d (Purple bars). Assays performed in triplicate and plotted as mean + SD. Data shown is representative replicate (N=3). All data normalised to no drug control (black bars). Statistics determined by two-way ANOVA with multiple comparisons against the no drug control. *, $0.05 \geq P > 0.01$; **, $0.01 \geq P > 0.001$; ***, $0.001 \geq P > 0.0001$; ****, $P \leq 0.0001$.

(d) Replication kinetics of SARS-CoV-2 WT and ΔCS viruses in HAE cells. Cells were pretreated with control media or media containing camostat for 1 hour then infected at an MOI of 0.1. Assays performed in triplicate and plotted as mean + SD. Statistics were determined by one-way ANOVA with multiple comparisons on log transformed data. Black P-values indicate statistical significance between no drug controls of WT and ΔCS while coloured P-values indicate significance between no drug control or camostat.

(e,f,g,h) Gene expression of select SARS-CoV-2 entry factors in (e) 293T-ACE2, (f) Caco-2, (g) Calu-3 or (h) HAEs. Gene expression determined by qRT-PCR and normalised to *β-actin*. Assays performed in triplicate and plotted as mean + SD. Data shown is representative replicate (N=2), except primary HAEs, where data points represent repeats in (N=3) independent donors.

Figure 3. The efficient furin cleavage site-dependent entry of SARS-CoV-2 is due to TMPRSS2 and allows for subsequent escape from IFITM3.

(a) Relative lentiviral pseudotype (PV) entry into 293T cells expressing ACE2-FLAG with or without co-expression of TMPRSS2. Entry into cells not transfected with TMPRSS2 normalised to 1. Assays performed in triplicate and plotted as mean + SD. Data shown is representative replicate (N=4). Statistics determined by multiple t-tests. ****, $P \leq 0.0001$.

(b,c) Replication kinetics of SARS-CoV-2 WT and ΔCS viruses in (b) Vero E6 and (c) Vero E6/TMPRSS2 cells at an MOI of 0.1. Assays performed in triplicate and plotted as mean + SD. Statistics were determined by one-way ANOVA with multiple comparisons on log transformed data.

(d,e,f) Relative PV entry into (d) 293T-ACE2, (e) Caco-2 or (f) Calu-3 cells pretreated with Amphotericin B (pink bars). Entry into untreated cells normalised to 1 (black bars). Assays performed in triplicate and plotted as mean + SD. Data shown is representative replicate (N=4). Statistics determined by multiple two-tailed t-tests. *, $0.05 \geq P > 0.01$; **, $0.01 \geq P > 0.001$

(g) Relative PV entry into 293T cells overexpressing ACE2-FLAG and TMPRSS2, with or without IFITM3. Entry into cells not transfected with IFITM3 normalised to 1 (black bars). Assays performed in triplicate and plotted as mean + SD. Data shown is representative replicate (N=4). Statistics determined by multiple two-tailed t-tests. **, $0.01 \geq P > 0.001$; ***, $0.001 \geq P > 0.0001$; ****, $P \leq 0.0001$.

(h,i) Replication kinetics of SARS-CoV-2 WT and ΔCS viruses in (h) Calu-3 or (i) HAE cells. Cells were pretreated with control media or media containing amphotericin B for 1 hour then infected at an MOI of 0.05 (Calu-3) or 0.1 (HAE). Assays performed in triplicate and plotted as mean + SD. HAE assay performed with three separate donor with data from representative donor shown. Statistics were determined by one-way ANOVA with multiple comparisons on log transformed data. Black P-values indicate statistical significance between no drug controls of WT and ΔCS while coloured P-values indicate significance between no drug control or amphoB. Vehicle controls were the same as from Figure 3D.

Figure 4. The furin cleavage site of SARS-CoV-2 allows for efficient replication and transmission in a ferret model

(a, b) Head to head transmission experiment of SARS-CoV-2 mix of WT and ΔCS in ferrets. In each group four individually housed donor ferrets were infected with X pfu of either WT or ΔCS SARS-CoV-2. One day post-inoculation naïve contact ferrets were added to each donor ferret. Ferrets were sampled by nasal wash daily and direct contact (A) and contact (B) ferret virus titres were determined by E gene qPCR. Statistics were determined by multiple two-tailed t tests of the log transformed E gene copy numbers between each group. *, 0.05 ≥ P

(c,d) Competition transmission experiment of SARS-CoV-2 mix of WT and ΔCS in ferrets. Four individually housed donor ferrets (c) were infected with 10^5 pfu of virus mix containing ~70% ΔCS and ~30% WT. One day post-inoculation naïve contact ferrets (d) were added to each donor ferret. Ferrets were sampled by nasal wash daily and virus titres were determined by E gene qPCR. For donors on day 2, 3, 5, 6 and 8, and for contacts on day 3, 6, 8 and 9 viral RNA across the S1/S2 cleavage site was deep sequenced. Where sequencing data was obtained bars showing the ratio of WT and deletion are shown.

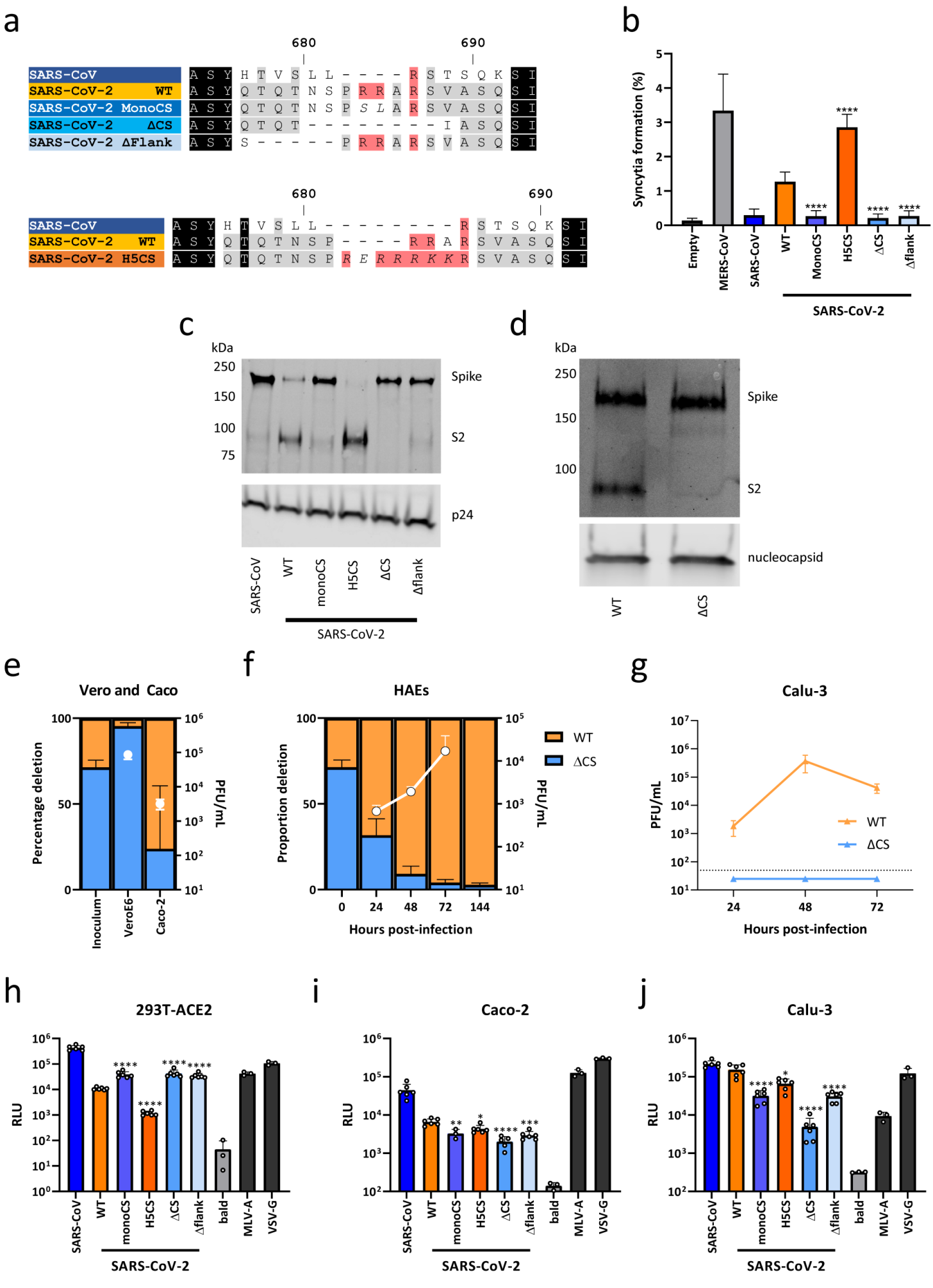
a
680
690
SARS-CoV
SARS-CoV-2 WT
SARS-CoV-2 MonoCS
SARS-CoV-2 ΔCS
SARS-CoV-2 ΔFlank
A S Y H T V S L L - - - - R S T S Q K S I
A S Y Q T Q T N S P R R A R S V A S Q S I
A S Y Q T Q T N S P S L A R S V A S Q S I
A S Y Q T Q T - - - - - - - I A S Q S I
A S Y S - - - - - P R R A R S V A S Q S I
680
690
SARS-CoV
SARS-CoV-2 WT
SARS-CoV-2 H5CS
A S Y H T V S L L - - - - - - - - R S T S Q K S I
A S Y Q T Q T N S P - - - - R R A R S V A S Q S I
A S Y Q T Q T N S P R E R R R K K R S V A S Q S I
b
Syncytia formation (%)
Empty
MERS-CoV
SARS-CoV
WT
MonoCS
H5CS
ΔCS
Δflank
SARS-CoV-2
c
kDa
250
150
100
75
Spike
S2
p24
SARS-CoV
WT
monoCS
H5CS
ΔCS
Δflank
SARS-CoV-2
d
kDa
250
150
100
Spike
S2
nucleocapsid
WT
ΔCS
e
Vero and Caco
Percentage deletion
PFU/mL
Inoculum
VeroE6
Caco-2
f
HAEs
Proportion deletion
PFU/mL
WT
ΔCS
Hours post-infection
g
Calu-3
PFU/mL
WT
ΔCS
Hours post-infection
h
293T-ACE2
RLU
SARS-CoV
WT
monoCS
H5CS
ΔCS
Δflank
bald
MLV-A
VSV-G
SARS-CoV-2
i
Caco-2
RLU
SARS-CoV
WT
monoCS
H5CS
ΔCS
Δflank
bald
MLV-A
VSV-G
SARS-CoV-2
j
Calu-3
RLU
SARS-CoV
WT
monoCS
H5CS
ΔCS
Δflank
bald
MLV-A
VSV-G
SARS-CoV-2

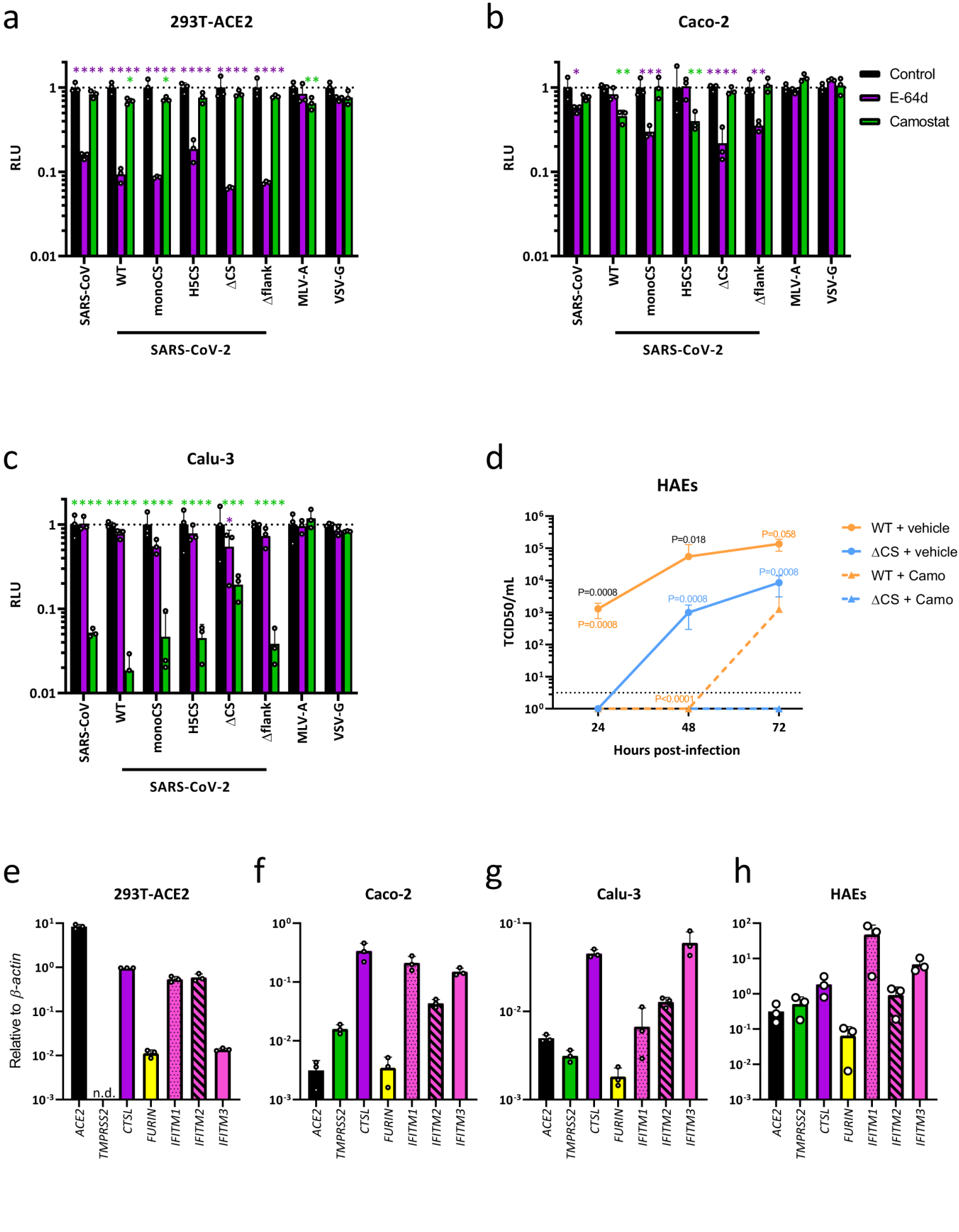
a
293T-ACE2
RLU
SARS-CoV
WT
monoCS
H5CS
ΔCS
Δflank
MLV-A
VSV-G
SARS-CoV-2
b
Caco-2
Control
E-64d
Camostat
c
Calu-3
d
HAEs
TCID50/mL
Hours post-infection
WT + vehicle
ΔCS + vehicle
WT + Camo
ΔCS + Camo
P=0.0008
P=0.018
P=0.058
P=0.0008
P=0.0008
P=0.0008
P<0.0001
e
293T-ACE2
Relative to β-actin
n.d.
f
Caco-2
g
Calu-3
h
HAEs
ACE2
TMPRSS2
CTSL
FURIN
IFITM1
IFITM2
IFITM3

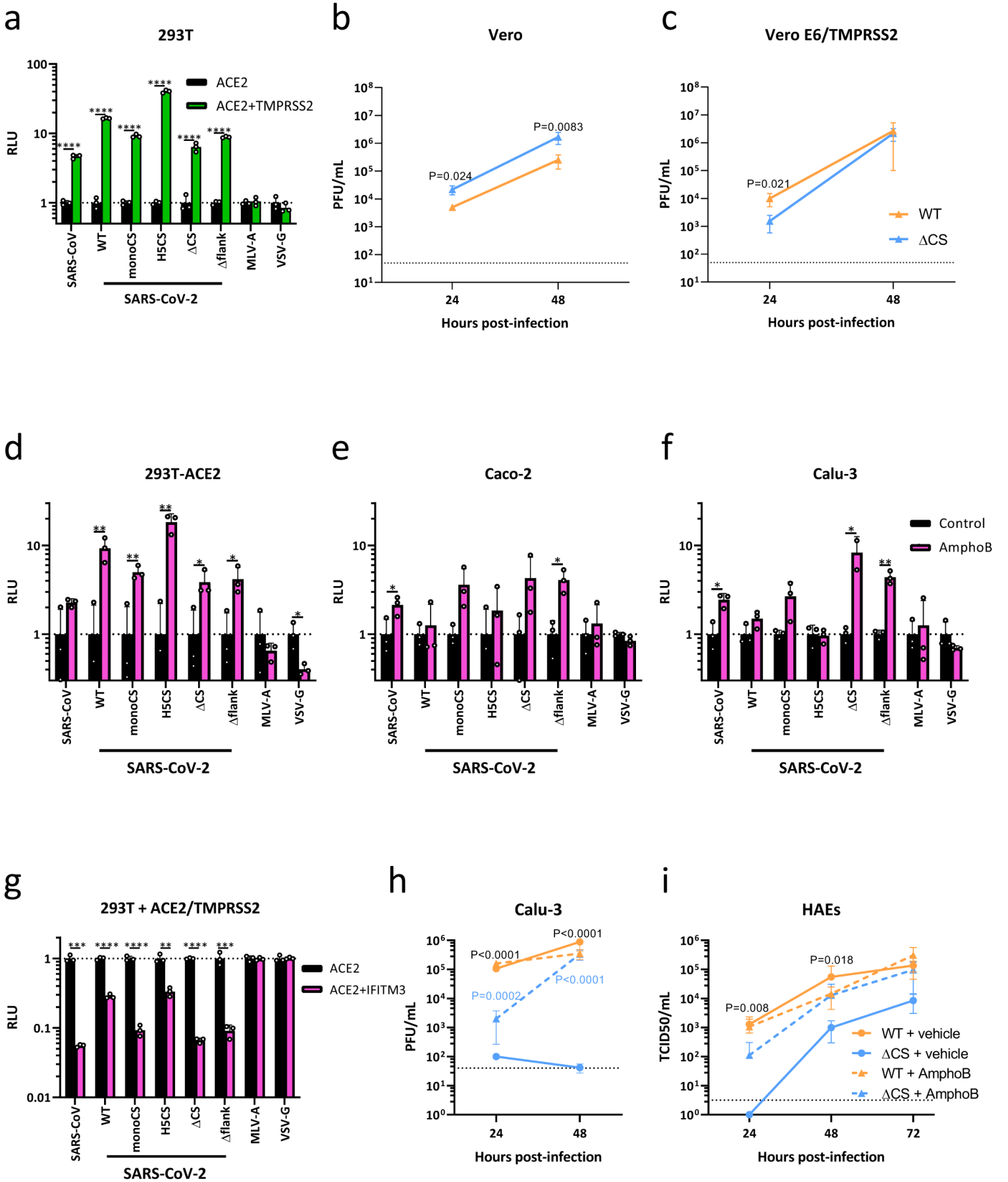
a
293T
RLU
ACE2
ACE2+TMPRSS2
SARS-CoV
WT
monoCS
H5CS
ΔCS
Δflank
MLV-A
VSV-G
SARS-CoV-2
b
Vero
PFU/mL
P=0.0083
P=0.024
24
48
Hours post-infection
c
Vero E6/TMPRSS2
PFU/mL
P=0.021
WT
ΔCS
24
48
Hours post-infection
d
293T-ACE2
RLU
SARS-CoV-2
e
Caco-2
RLU
SARS-CoV-2
f
Calu-3
RLU
Control
AmphoB
SARS-CoV-2
g
293T + ACE2/TMPRSS2
RLU
ACE2
ACE2+IFITM3
SARS-CoV-2
h
Calu-3
PFU/mL
P<0.0001
P<0.0001
P<0.0001
P=0.0002
24
48
Hours post-infection
i
HAEs
TCID50/mL
P=0.018
P=0.008
WT + vehicle
ΔCS + vehicle
WT + AmphoB
ΔCS + AmphoB
24
48
72
Hours post-infection

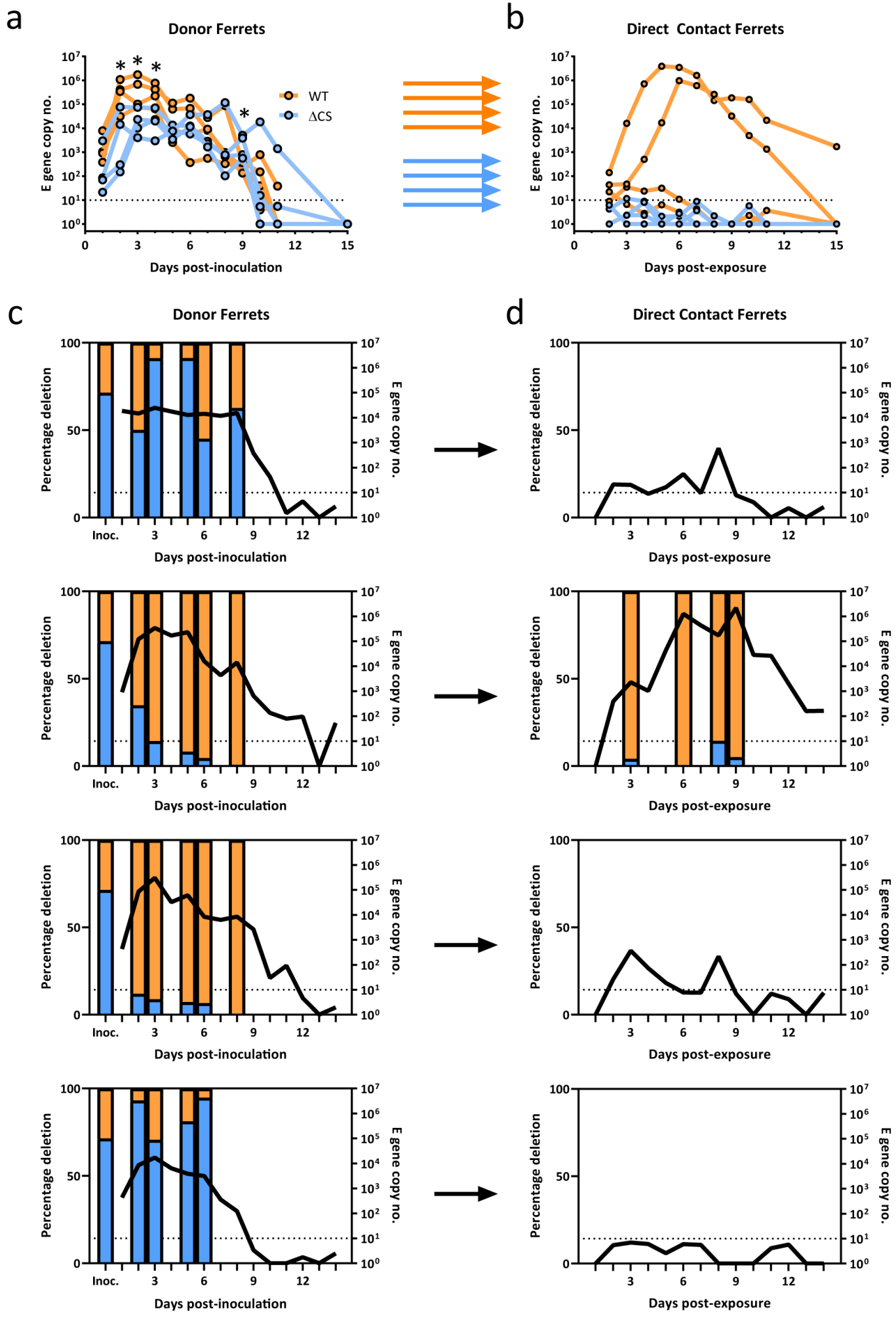
a
Donor Ferrets
E gene copy no.
Days post-inoculation
WT
ΔCS
b
Direct Contact Ferrets
E gene copy no.
Days post-exposure
c
Donor Ferrets
Percentage deletion
E gene copy no.
Inoc.
Days post-inoculation
d
Direct Contact Ferrets
Percentage deletion
E gene copy no.
Days post-exposure